PCCP

PAPER

View Article Online
View Journal | View Issue

Melt-infiltration of spiro-OMeTAD and thermal instability of solid-state dye-sensitized solar cells†

Cite this: *Phys. Chem. Chem. Phys.*, 2014, **16**, 4864

Colin D. Bailie,[a] Eva L. Unger,[a] Shaik M. Zakeeruddin,[b] Michael Grätzel[b] and Michael D. McGehee*[a]

Received 15th October 2013,
Accepted 10th January 2014

DOI: 10.1039/c4cp00116h

www.rsc.org/pccp

A method for achieving complete pore-filling in solid-state dye-sensitized solar cells termed melt-infiltration is presented: after the customary solution-processed deposition of spiro-OMeTAD, the device is heated above the glass transition temperature of spiro-OMeTAD to soften the material and allow capillary action to pull additional spiro-OMeTAD from the overlayer reservoir into the pores. The pore-filling fraction increases from 60–65% to 90–100% as a result of melt-infiltration. The organic D–π–A dye used in this study is found to withstand the thermal treatment without performance loss, unlike ruthenium-based dyes. Through our experiments, we find that the 4-*tert*-butylpyridine (*t*BP) additive, commonly used in dye-sensitized solar cells, evaporates from the device during heat treatment at temperatures as low as 85 °C. This significantly impacts device performance, potentially excluding its use in commercial applications, and demonstrates the need for a more thermally stable *t*BP alternative. Melt-infiltration is expected to be a viable method for achieving complete pore-filling in systems where volatile additives are not required for operation.

Introduction

Solid-state dye-sensitized solar cells[1] (ssDSSCs) are competitive alternatives to liquid dye-sensitized solar cells[2] with demonstrated efficiencies of 7.2%.[3] ssDSSCs are fabricated by sensitization of a mesoporous scaffold of TiO_2 nanoparticles with light absorbing dye molecules followed by solution-deposition of an organic hole-transporting material to fill the pore volume of TiO_2.

Currently, optimal device thicknesses of around 2 μm are reached by a tradeoff between light absorption and charge collection efficiency.[4] The latter is in part limited by incomplete pore-filling of the meso-porous titania scaffold by the organic hole-transporting material, such as 2,2′,7,7′-tetrakis(*N*,*N*-di-*p*-methoxyphenylamine)-9,9-spirobifluorene (spiro-OMeTAD).[5,6] The degree of pore-filling is expressed as the pore-filling fraction (PFF) which is the ratio of the volume of the spiro-OMeTAD within the TiO_2 pores to the total volume of the TiO_2 pores. Ding *et al.* demonstrated that deposition of spiro-OMeTAD from a chlorobenzene solution by either doctor-blading or spin-coating onto a porous TiO_2 film is limited to a 60–65% PFF and decreases with increasing TiO_2 thickness.[5,7] Melas-Kyriazi *et al.* demonstrated that pore-filling of spiro-OMeTAD is an important factor in determining essential device metrics such as hole-injection efficiency, charge recombination lifetime, electron diffusion length, and charge collection efficiency. They estimated that an improvement in the PFF from 65% to 100% would provide an immediate relative efficiency improvement in a 2 μm ssDSSC of around 5%. Additionally, they estimated that the optimal meso-porous TiO_2 layer thickness could be increased from 2 μm to 5 μm, if the PFF at 5 μm could be increased from currently 40%[5] to 100%. This would lead to a substantial increase in light absorption and a 25% relative efficiency improvement compared to a state-of-the-art 2 μm ssDSSC with a 65% PFF.[6] Margulis *et al.* found that the oxidized form of spiro-OMeTAD, which is necessary for appreciable conductivity of the material, competes strongly with the dye molecules for absorption of light across the entire visible spectrum.[8] Additional parasitic absorption by the spiro-OMeTAD upon increasing the PFF was not considered in the estimations by Melas-Kyriazi *et al.*

Multiple attempts have been made to improve the PFF of small organic molecules in TiO_2 nanostructures for ssDSSCs. Fredin *et al.* introduced low melting-point hole-transporters *via* drop-casting from solution or application of the hole-transporter in powder form and subsequently melting the materials.[9,10] Juozapavicius *et al.* used a melt-processed hole-conductor and doped it with iodine vapor.[11] However, in no examples of melt-infiltration has the efficiency surpassed 0.12% at 1 sun intensity, nor has a 100% PFF been measured.

[a] *Department of Materials Science and Engineering, Stanford University, Stanford, CA 94305, USA. E-mail: mmcgehee@stanford.edu*

[b] *Laboratoire de Photoniques et Interfaces, Institut des Sciences et Ingénierie Chimiques, École Polytechnique Fédérale de Lausanne, Station 6, 1015 Lausanne, Switzerland*

† Electronic supplementary information (ESI) available. See DOI: 10.1039/c4cp00116h

Additionally, the strategies employed to melt-process these hole-transporters provide very little control of the solid hole-transport overlayer thickness, which in highly efficient ssDSSCs is an important factor in controlling the internal series resistance. In an alternative strategy, Leijtens *et al.* used highly soluble hole transporting materials with the aim of surpassing the solution-limited pore-filling fraction of 65%, but the overall device efficiency was reduced due to the lower charge carrier mobility of this material compared to spiro-OMeTAD.[12]

Spiro-OMeTAD is the material of choice for highly performing ssDSSCs with a good combination of processability and charge carrier mobility. Improving the PFF of spiro-OMeTAD is therefore a promising route for device improvement. In this report we demonstrate a 100% PFF of spiro-OMeTAD in a mesoporous TiO_2 film with controlled overlayer thickness by melt-infiltration. We find that devices subjected to melt-infiltration suffer from severe performance degradation at processing temperatures as low as 85 °C. We identify the volatility of the common additive 4-*tert*-butylpyridine (*t*BP) as a factor causing major performance degradation during thermal processing and thermal stressing of ssDSSCs. Because 85 °C is standard for thermal stress testing of solar cells in commercial applications,[13] a stable replacement for *t*BP must be found to achieve long-term stability of solid state dye sensitized solar cells.

Melt-infiltration

Spiro-OMeTAD has a glass transition temperature of 125 °C and a melting temperature of 248 °C.[12] Above the glass transition temperature, spiro-OMeTAD exists as an amorphous glass, exhibiting viscoelastic behavior. As is common in glass-forming materials,[14] the viscosity is high just above the glass transition temperature but can be substantially reduced by increasing the temperature further. Glasses have a low enough viscosity to exhibit macroscopic flow on the timescale of minutes at an appropriately high temperature. 150 °C was found in this study to be sufficiently above the glass transition temperature such that the melt-infiltration process could be completed within 30 min. Alternatively, spiro-OMeTAD may be processed as a liquid, with the advantage that a liquid has many orders of magnitude lower viscosity than a viscous glass, and infiltrates more quickly. In its liquid state, spiro-OMeTAD was found to show flow behavior similar to a viscous oil. A hotplate temperature well above the melting point, 280 °C, was chosen for this study in order to account for both thermal contact resistance at the hot plate-sample interface and convective heat transfer at the sample surface, which could cause the sample surface to be cooler than the hotplate. Spiro-OMeTAD deposited as a powder on a glass slide was found to become completely liquid within 2 s at 280 °C.

The method for measuring pore-filling fraction was developed by Ding *et al.*[5] and is described here briefly. The pore-filling fraction can be simply stated as the volume of spiro-OMeTAD in the TiO_2 pores divided by the total pore volume available. The total pore volume of TiO_2 is determined by multiplying the thickness of the TiO_2 film, obtained *via* scanning electron microscopy (SEM), by the sample area, and the porosity. By BET analysis, the porosity of the TiO_2 film is found to be 0.68, which is reduced to 0.476 when dyed with Z907.[15] The total spiro-OMeTAD volume is determined spectroscopically using Beer's law and the previously reported molar extinction coefficient of spiro-OMeTAD ($\varepsilon(\lambda = 389\ \text{nm}) = 74\,700\ \text{M}^{-1}\ \text{cm}^{-1}$)[5] along with its molar mass (1225.4 g mol^{-1}) and its density ($\rho = 1.82\ \text{g cm}^{-3}$).[5] The volume of the spiro-OMeTAD overlayer on top of the TiO_2 is accounted for by measuring the overlayer thickness using SEM prior to dissolving the spiro-OMeTAD in chlorobenzene.

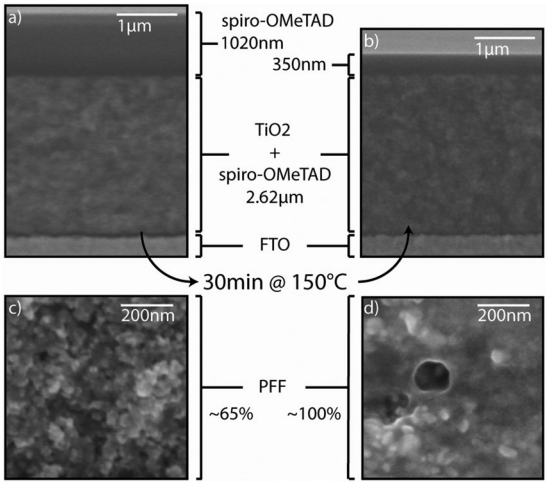

Fig. 1 Visual example of the effect of melt-infiltration. (a) A sample with spin-coated spiro-OMeTAD is heated for 30 min at 150 °C to yield (b) a sample with significantly reduced spiro-OMeTAD overlayer thickness. Spiro-OMeTAD in the overlayer is pulled into the mesoporous TiO_2 structure, improving the pore-filling. (c) A high-magnification SEM image of a 65% PFF sample contrasts significantly with (d) a high-magnification SEM image of a 100% PFF sample.

Spiro-OMeTAD was first deposited onto a dye-sensitized TiO_2 film following a standard procedure by spin-coating in air. Initial deposition of the spiro-OMeTAD by this method allows for precise engineering of the final overlayer thickness after melt-infiltration, allowing devices to be fabricated with a desired overlayer chosen to balance shunt resistance against series resistance. After drying the films, melt-infiltration was performed in a nitrogen glovebox in the dark. Samples were heated at either 150 °C for 30 min or 280 °C for 30 s. During melt-infiltration, additional spiro-OMeTAD from the overlayer infiltrates the mesoporous TiO_2 film. This is clearly visible as a decrease in overlayer thickness (Fig. 1). The PFF of films before melt-infiltration was found to be 63%, in agreement with the 60–65% PFF limitation by solution deposition found by Ding *et al.*[5] As shown in Table 1, heating the spiro-OMeTAD to a glassy state was found to improve the PFF to a maximum of 99% with an average of 88%. Melting the spiro-OMeTAD to a liquid was found to improve the PFF to a maximum of 100%‡

‡ Measuring a 100% PFF denotes the quantitative accuracy of this measurement method and calls into question the absolute values determined by indirect measurement techniques such as equivalent layer thickness[27] and optical reflectometry.[28]

Table 1 Measured pore-filling fraction values and overlayer thicknesses of melt-infiltrated films

Case	Room temp control[a]	30 min at 150 °C[b]	30 s at 280 °C[b]
Average PFF	63%	88%	94%
Standard deviation of the PFF		10%	5%
Maximum PFF		99%	100%

By propagation of error, individual PFF measurements have a random uncertainty of ±4.5%. [a] Sample set of 2 films. [b] Sample set of 6 films.

Table 2 Effect of subjecting D35-sensitized ssDSSCs to heat prior to spiro-MeOTAD deposition

Case (D35 heat treatment before spiro)	J_{sc} (mA cm^{-2})	V_{oc} (V)	Efficiency (%)	FF (−)
No heat treatment[a]	5.78	0.73	2.27	0.54
150 °C for 30 min before spiro[b]	6.38	0.72	2.93	0.64
280 °C for 30 s before spiro[b]	5.39	0.70	2.44	0.65

[a] Average of 18 devices. [b] Average of 9 devices.

with an average of 94%. By propagation of error, random uncertainty in the PFF of individual measurements was found to be ±4.5%. Systematic uncertainty caused by errors in published constants such as the TiO_2 porosity or the density of spiro-OMeTAD is not considered. Spiro-OMeTAD overlayer thickness after melt-infiltration within a film was controlled to ±30 nm, and the variance of average overlayer thickness between films was ±30–40 nm. Such film uniformity and reproducibility were found to be similar to the overlayers of spin-coated films prior to melt-infiltration. No crystallization of the spiro-OMeTAD was observed by optical microscopy as a result of the melt-infiltration process.

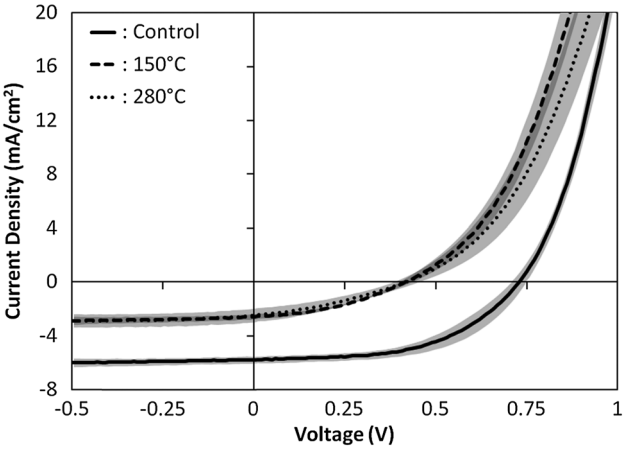

Fig. 2 *I–V* curves of devices subjected to melt-infiltration compared to controls not subjected to melt-infiltration. Solid lines represent the average of individual devices, faded area represents the ±1 standard deviation in current density at each voltage step.

Solid-state dye-sensitized solar cells

A major concern for melt-infiltration in a complete device is the thermal stability of the dye molecule, which may be prone to decomposition or desorption from the TiO_2 surface at elevated temperature. A study by Fredin *et al.* demonstrated that an organic D–π–A type dye (D5) displayed a better thermal stability compared to a ruthenium dye (N719).[16] To ensure that the dye used in this study, D35, would be thermally stable during melt-infiltration, dye-sensitized TiO_2 films were subjected to the temperatures used for melt-infiltration in a nitrogen atmosphere prior to spiro-OMeTAD deposition. The performance of these devices, shown in Table 2, indicates that the dye is thermally stable to the heating conditions imposed during melt-infiltration.

Devices were made to test the effect of melt-infiltration and the increased PFF on performance by thermally treating the devices after spiro-OMeTAD deposition by spin-coating. We observed a substantial decrease in short-circuit current (J_{SC}), open-circuit voltage (V_{OC}) and the fill factor (FF) as a result of melt-infiltration (Table S1 in the ESI† and illustrated in Fig. 2).

Considering that the dye-sensitized TiO_2 films were found to be stable during the thermal conditions of melt-infiltration, we interpret the decrease in device performance during melt-infiltration to be caused by changes to the hole-transport layer. A possible explanation is a change in the additive composition of the hole-transport layer. Aside from spiro-OMeTAD, the hole-transport layer includes bis(trifluoromethane)sulfonimide lithium salt (Li-TFSI) and *tert*-butylpyridine (*t*BP). Li-TFSI has been shown to catalyze a complex doping mechanism involving oxygen in which oxidized spiro-OMeTAD is formed and Li-TFSI is consumed.[17] The TFSI counter-ion probably stabilizes spiro-OMeTAD$^+$. While the oxygen content in the nitrogen glovebox was kept below 5 ppm during melt-infiltration, the elevated temperatures may nevertheless significantly increase reaction rates such that Li-TFSI was consumed during melt-infiltration. Since the melt-infiltrated devices shown in Fig. 2 did not demonstrate a decrease in series resistance, it is unlikely that the Li-TFSI is being consumed. *t*BP is a volatile organic molecule and has a boiling point of 197 °C. While melt-infiltration at 150 °C is below the boiling point of *t*BP, if *t*BP possesses an appreciable equilibrium partial pressure at this temperature it may evaporate during the melt-infiltration process due to the high surface area of TiO_2 and the small quantities of *t*BP present in the system.

*t*BP plays several essential roles in ssDSSCs. *t*BP aids in dissolving the essential Li-TFSI additive in the spiro-OMeTAD solution.[18] However, since the *t*BP was present during deposition, this role can be considered completed before melt-infiltration occurs. In devices, *t*BP influences the interfacial energetics at the dye–TiO_2 interface by shifting the TiO_2 conduction band to more negative potentials (with respect to NHE).[19,20] If adsorbed to the TiO_2 surface in the vicinity of and in-between the sensitizer–dye molecules, *t*BP can influence the absorption spectrum, especially of D–π–A dyes, by a Stark effect exerted by their local electric field.[21,22] Changes in interfacially adsorbed *t*BP concentrations affect the absorption spectra of the dye. Removal of *t*BP is found to significantly reduce both J_{SC} and V_{OC}.[18] These observations are consistent

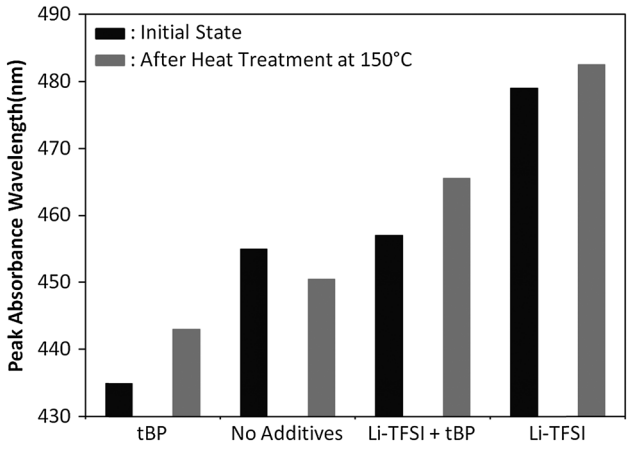

Fig. 3 Peak wavelength of solid-state absorbance of D35-dyed TiO_2 films with varying additives present in the film introduced during spiro-OMeTAD deposition. The effect of heating the films to 150 °C is shown.

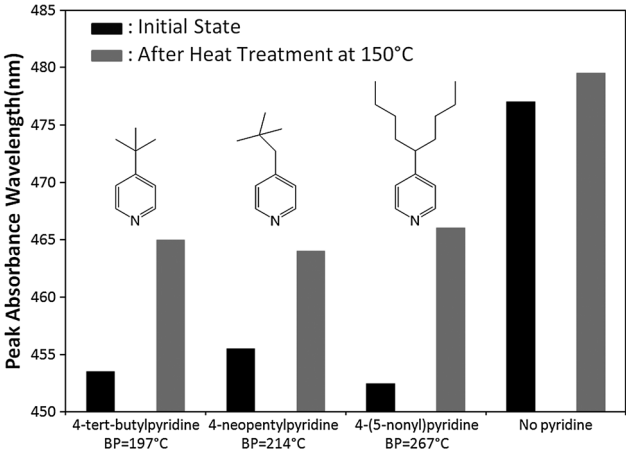

Fig. 4 Peak wavelength of solid-state absorbance D35-dyed TiO_2 films dyed with spiro-OMeTAD, Li-TFSI and varying pyridines present in the film. The effect of heating the films to 150 °C is shown. Pyridine structures are shown above corresponding columns.

with the effect of melt-infiltration on ssDSSC performance and further support the hypothesis that *t*BP evaporation is a major source of device performance degradation during melt-infiltration.

It is possible therefore to probe for the presence of additives at the TiO_2 surface by analyzing the absorption spectra of the films. Specifically, it was found that compared to the spectrum of D35 on TiO_2, the presence of *t*BP blue-shifts the absorption peak of the main absorption band of D35 while the presence of Li-TFSI red-shifts the absorption peak of the main absorption band, and the presence of both Li-TFSI and *t*BP was found to have offsetting effects on the D35 absorption spectrum (see black columns of Fig. 3).

When films containing *t*BP were heated, the absorption peak red-shifted by approximately 8 nm, as one would expect if some *t*BP left the TiO_2 interface (Fig. 3). In contrast, the absorption peak did not change as much for films not containing *t*BP. Similar results were found when heating films not containing spiro-OMeTAD (see Fig. S1, ESI†). In addition to corroborating the conjecture that *t*BP is leaving the TiO_2 interface during heating, the results for films not containing spiro-OMeTAD exclude the possibility that *t*BP is dissolved in the spiro-OMeTAD matrix instead of fully evaporating from the film since the only option for *t*BP to leave the TiO_2 surface in this case is to evaporate. The absence of large peak shifts for films containing only the Li-TFSI as an additive indicates the thermal stability of the Li-TFSI additive.

Since evaporation of the pyridine additive at elevated temperature causes device degradation during melt-infiltration, alternative pyridines with higher boiling points were employed to try to mitigate this degradation mechanism. While the boiling point (BP) of *t*BP is 197 °C, pyridine alternatives exist with appreciably higher boiling points. The boiling point of 4-neopentyl pyridine is 214 °C and the boiling point of 4-(5-nonylpyridine) is 267 °C. However, during melt-infiltration (as shown in Fig. 4) these higher boiling point pyridines were found to behave identically to *t*BP. This finding indicates that the pyridine can evaporate from the system at temperatures more than 100 °C and less than the boiling point of the pyridine.

In addition to the melt-infiltration procedure attempted herein, methods designed for reintroducing the *t*BP, forcing the *t*BP to remain in the device, and low-temperature methods for increasing the PFF were attempted. Solvent annealing the device in an atmosphere of various organic solvents was attempted on the premise that introducing organic solvents *via* the vapor phase would soften the spiro-OMeTAD layer, lowering the glass transition to room temperature and allowing capillary forces to pull the spiro-OMeTAD into the pores. However, this strategy was found to have detrimental effects on the spiro-OMeTAD overlayer such as inducing crystallization or causing beading of the spiro-OMeTAD rather than filling the pores more completely. In a similar vein, *t*BP was reintroduced to the ssDSSC after melt-infiltration *via* vapor phase, but similar to solvent annealing with other solvents, detrimental effects on the spiro-OMeTAD overlayer were observed with no indication *via* absorption spectroscopy that *t*BP successfully reached the TiO_2 surface. Limiting the ability of *t*BP to evaporate was attempted by either capping with a Ag electrode or by pressing a fluorinated polymer film (*e.g.* polytetrafluoroethylene) with 2.5×10^7 Pa or 250 atm of pressure onto the spiro-OMeTAD during melt-infiltration. In the case of pressing the fluorinated polymer film during melt-infiltration it was found that the spiro-OMeTAD film plastically deformed by shearing when the polymer film was removed. When capped with a Ag electrode, the Ag electrode was observed to buckle and crack, likely caused by a low buckling resistance due to the high aspect ratio of the electrode coupled with a lack of mechanical support from the spiro-OMeTAD layer underneath which is viscous during melt-infiltration.

Thermal stress testing of ssDSSCs

Since this study revealed that a volatile pyridine additive like *t*BP can evaporate from the ssDSSC at temperatures significantly below the boiling point, we became concerned that even

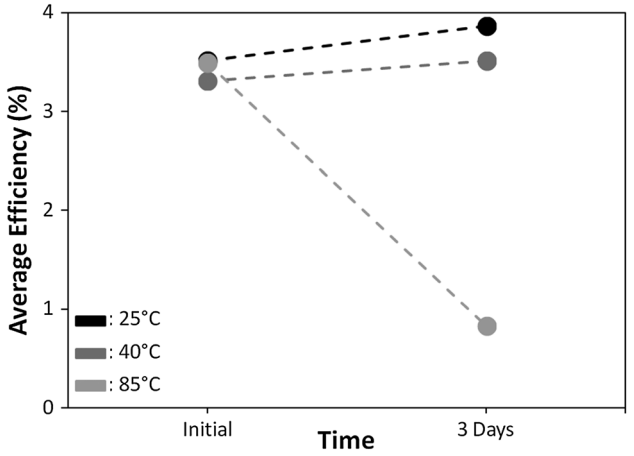

Fig. 5 Change in efficiency over time of devices subjected to varying thermal stress temperatures in a nitrogen glovebox in the dark over 3 days. Each case is an average of 2 devices. Dashed lines are a guide to the eye.

cells made without melt-infiltration would degrade at 85 °C,[13] a temperature that can be encountered in outdoor environments and is used in standardized solar cell device stress testing. To test the volatility of *t*BP at elevated operating temperatures, devices were fabricated and tested then heated in the dark in a nitrogen glovebox over three days then re-tested. Results shown in Fig. 5 clearly demonstrate that while the ssDSSC is stable to the moderate temperatures of 25 °C and 40 °C, devices quickly degrade at 85 °C. Solid-state absorption measurements before and after heating show a 6 nm red-shift of the D35 maximum absorption peak of the samples heated to 85 °C. This is in accordance with our observation of samples subjected to melt-infiltration conditions. Evaporation of *t*BP and other volatile components from the devices will over time lead to a change in composition and performance of the solar cell devices. We emphasize that evaporation of *t*BP may not be the only degradation process during melt-infiltration and thermal stressing of ssDSSCs and that other degradation mechanisms may also be occurring. Among those, we consider that changes in the spiro-OMeTAD morphology such as crystallization within the pores could disrupt percolation to the back electrode, causing morphological hole traps. No spiro-OMeTAD crystallization was observed by optical microscopy in these experiments. Though nano-crystallization within the TiO_2 pores may still occur during heating, investigation of these organic crystals is beyond the scope of this work.

Experimental details

For solar cell experiments, fluorine-doped tin oxide glass substrates (TEC15, Hartford Glass Co.) were patterned by etching with zinc powder (J. T. Baker) and 2 M hydrochloric acid (Aldrich). After cleaning the substrates by ultrasonication in water and a UV/ozone treatment, a compact TiO_2 layer was deposited by spray pyrolysis of titanium bis(acetylacetonate)diisopropoxide solution (Aldrich) dissolved in ethanol (in 1 : 10 volume ratio) at 450 °C using oxygen as a carrier gas. A mesoporous TiO_2 layer 1.7–1.8 μm thick was then deposited on the substrates by screen-printing, dried at 125 °C, gradually heated to 500 °C, and then baked at this temperature for 15 min. After cooling to room temperature, the substrates were treated in a 0.02 M aqueous solution of $TiCl_4$ (Aldrich) for 18 h at room temperature. Synthesis of the TiO_2 colloid (basic route) was performed according to the report by Barbé *et al.*[23] A paste was prepared from the TiO_2 colloid according to the report by Ito *et al.*[24] Brunauer–Emmett–Teller (BET) surface area analysis was utilized to determine an average particle size of 23 nm, an average pore diameter of 32 nm and a film porosity of 0.68. Prior to sensitization, the TiO_2 substrates were heated to 500 °C for 30 min. After cooling to ~70 °C, the substrates were immersed into a 0.2 mM solution of the sensitizer, D35 (Dyenamo),[25] in ethanol overnight followed by rinsing in acetonitrile and drying with compressed nitrogen. The hole-transporting material was deposited by spin-coating at 2000 rpm for 30 s. The formulation of the spin-coating solution was 300 mg spiro-OMeTAD (Luminescence Technology Corp., LT-S922), 62.5 μL lithium bis-(trifluoromethylsulfonyl)imide (Li-TFSI) (Aldrich) pre-dissolved as a 170 mg mL^{-1} solution in acetonitrile, and 29.2 μL 4-*tert*-butylpyridine(*t*BP) (Aldrich) in 1 mL chlorobenzene. For thermal stability experiments, the concentrations of spiro-OMeTAD, *t*BP, and Li-TFSI were reduced by 25%. Finally, 200 nm of silver was thermally evaporated on top of the device to form the back contact. Testing was performed in ambient air to allow the spiro-OMeTAD film to become doped by oxidation. *J–V* curves were generated using a Keithley 2400 source meter, and an AM 1.5G solar simulator with a xenon lamp calibrated with a reference silicon diode.

For pore-filling experiments, the solar cell fabrication procedure was altered by removing the etching, spray pyrolysis, and $TiCl_4$ steps. In addition, a different sensitizer, Z907 (Dyesol, DNH2) was used in a 0.3 mM solution in a 1 : 1 by volume mixture of acetonitrile and *tert*-butanol. The films were dyed overnight. The hole-transporting material was applied after the dyeing step in the same procedure. The formulation of the spin-coating solution was 300 mg spiro-OMeTAD in 1 mL chlorobenzene and did not contain Li-TFSI or *t*BP additives because their volumetric contributions cannot be accounted for. After drying the films, melt-infiltration was performed in a nitrogen glovebox in the dark. Samples were heated at either 150 °C for 30 min or 280 °C for 30 s. The temperatures described in this study refer to the temperature measured on the surface of the hot plate. The temperature of the sample surface is expected to be slightly lower. Calculation of the pore-filling fraction utilized constants determined by Ding *et al.*[5] Porosity of Z907-dyed TiO_2 film is 0.476,[15] the molar extinction coefficient of spiro-OMeTAD at λ = 389 nm is 74 700 M^{-1} cm^{-1}, molar mass of spiro-OMeTAD is 1225.4 g mol^{-1}, and density of a spiro-OMeTAD film is 1.82 g cm^{-3}.

For absorption experiments, films were prepared using the same method as for solar cell experiments, excluding additives from the spiro-OMeTAD solution as indicated. For absorption experiments without spiro-OMeTAD, additives were introduced to the TiO_2 surface after dyeing by immersing the film in a solution containing additives for 2 min in a similar manner to

Zhu *et al.*[26] Additives were added to acetonitrile as dictated by experimental conditions in concentrations of 8.75 μL of *t*BP per 200 μL acetonitrile or 18.75 μL of Li-TFSI pre-dissolved as a 170 mg mL^{-1} solution in acetonitrile per 200 μL acetonitrile. Optical changes were observed to occur much more quickly than the total melt-infiltration time. Therefore, 5 min at 150 °C and 5 s at 280 °C were chosen to investigate interfacial changes. Solid-state absorption experiments were performed on a Cary-6000i UV-Visible-NIR spectrophotometer.

To check for the presence of spiro-OMeTAD crystallization, films were observed after melt-infiltration at 50× magnification under polarized light using a Nikon Eclipse E600 polarizing microscope. Crystals of spiro-OMeTAD exhibit clear birefringence.

Conclusions

Melt-infiltration of spiro-OMeTAD is demonstrated to be an effective method for achieving a 100% PFF while maintaining control of overlayer thickness using the preferred hole-transporter for high-efficiency ssDSSCs. To our knowledge, this is the first report of quantitative measurement of a 100% PFF of a solid material in ssDSSCs.

Unfortunately, performance improvements expected from achieving a 100% PFF were not realized due to the volatility of the additive *t*BP, which limits the ability to thermally process the hole-transport layer. Evaporation of *t*BP and other volatile components from the devices will over time lead to a change in composition and performance of the solar cell devices. In addition to being incompatible with melt-infiltration, *t*BP is shown to evaporate from ssDSSCs at an 85 °C thermal stress test temperature; such volatility could preclude its use in commercial ssDSSCs, which must be stable to elevated temperatures encountered in outdoor environments. For improved thermal processability and long-term thermal stability, alternatives to *t*BP must be developed. To ensure that evaporation does not occur, these additives would ideally be chemically bound to the TiO_2 surface.

Acknowledgements

This work was supported by the Office of Naval Research (ONR) under grant No. 000141110244. MG would like to thank the European Research Council (ECR) advanced grant agreement (no. 247404) funded under the ''MESOLIGHT'' project. We thank Jen Dionne for use of her spectrophotometer, Dr Peter Pechy, Dr Yella Aswani and Mr Pascal Comte for providing samples of 4-neopetylpyridine, 4-nonylpyridine and mesoporous TiO_2 film, respectively.

References

1 U. Bach, D. Lupo, P. Comte, J. Moser, F. Weissörtel, J. Salbeck, H. Spreitzer and M. Grätzel, *Nature*, 1998, **395**, 583–585.
2 B. O'Regan and M. Grätzel, *Nature*, 1991, **353**, 737–740.
3 J. Burschka, A. Dualeh, F. Kessler, E. Baranoff, N.-L. Cevey-Ha, C. Yi, M. K. Nazeeruddin and M. Grätzel, *J. Am. Chem. Soc.*, 2011, **133**, 18042–18045.
4 H. J. Snaith and L. Schmidt-Mende, *Adv. Mater.*, 2007, **19**, 3187–3200.
5 I.-K. Ding, N. Tétreault, J. Brillet, B. E. Hardin, E. H. Smith, S. J. Rosenthal, F. Sauvage, M. Grätzel and M. D. McGehee, *Adv. Funct. Mater.*, 2009, **19**, 2431–2436.
6 J. Melas-Kyriazi, I.-K. Ding, A. Marchioro, A. Punzi, B. E. Hardin, G. F. Burkhard, N. Tétreault, M. Grätzel, J.-E. Moser and M. D. McGehee, *Adv. Energy Mater.*, 2011, **1**, 407–414.
7 I.-K. Ding, J. Melas-Kyriazi, N.-L. Cevey-Ha, K. G. Chittibabu, S. M. Zakeeruddin, M. Grätzel and M. D. McGehee, *Org. Electron.*, 2010, **11**, 1217–1222.
8 G. Y. Margulis, B. E. Hardin, I.-K. Ding, E. T. Hoke and M. D. McGehee, *Adv. Energy Mater.*, 2013, **3**, 959–966.
9 K. Fredin, E. M. J. Johansson, T. Blom, M. Hedlund, S. Plogmaker, H. Siegbahn, K. Leifer and H. Rensmo, *Synth. Met.*, 2009, **159**, 166–170.
10 K. Fredin, E. M. J. Johansson, M. Hahlin, R. Schölin, S. Plogmaker, E. Gabrielsson, L. Sun and H. Rensmo, *Synth. Met.*, 2011, **161**, 2280–2283.
11 M. Juozapavicius, B. C. O'Regan, A. Y. Anderson, J. V. Grazulevicius and V. Mimaite, *Org. Electron.*, 2012, **13**, 23–30.
12 T. Leijtens, I.-K. Ding, T. Giovenzana, J. T. Bloking, M. D. McGehee and A. Sellinger, *ACS Nano*, 2012, **6**, 1455–1462.
13 M. O. Reese, S. A. Gevorgyan, M. Jørgensen, E. Bundgaard, S. R. Kurtz, D. S. Ginley, D. C. Olson, M. T. Lloyd, P. Morvillo, E. A. Katz, A. Elschner, O. Haillant, T. R. Currier, V. Shrotriya, M. Hermenau, M. Riede, K. R. Kirov, G. Trimmel, T. Rath, O. Inganäs, F. Zhang, M. Andersson, K. Tvingstedt, M. Lira-Cantu, D. Laird, C. McGuiness, S. (Jimmy) Gowrisanker, M. Pannone, M. Xiao, J. Hauch, R. Steim, D. M. DeLongchamp, R. Rösch, H. Hoppe, N. Espinosa, A. Urbina, G. Yaman-Uzunoglu, J.-B. Bonekamp, A. J. J. M. van Breemen, C. Girotto, E. Voroshazi and F. C. Krebs, *Sol. Energy Mater. Sol. Cells*, 2011, **95**, 1253–1267.
14 D. Turnbull, *Contemp. Phys.*, 1969, **10**, 473–488.
15 N. Papageorgiou, C. Barbe and M. Grätzel, *J. Phys. Chem. B*, 1998, **102**, 4156–4164.
16 K. Fredin, K. F. Anderson, N. W. Duffy, G. J. Wilson, C. J. Fell, D. P. Hagberg, L. Sun, U. Bach and S.-E. Lindquist, *J. Phys. Chem. C*, 2009, **113**, 18902–18906.
17 A. Abate, T. Leijtens, S. Pathak, J. Teuscher, R. Avolio, M. E. Errico, J. Kirkpatrik, J. M. Ball, P. Docampo, I. McPherson and H. J. Snaith, *Phys. Chem. Chem. Phys.*, 2013, **15**, 2572–2579.
18 J. Krüger, PhD thesis, École Polytech. Fédérale Lausanne, 2003.
19 J. Krüger, R. Plass, L. Cevey, M. Piccirelli, M. Grätzel and U. Bach, *Appl. Phys. Lett.*, 2001, **79**, 2085.
20 S. A. Haque, Y. Tachibana, R. L. Willis, J. E. Moser, M. Grätzel, D. R. Klug and J. R. Durrant, *J. Phys. Chem. B*, 2000, **104**, 538–547.

21 S. Ardo, Y. Sun, F. N. Castellano and G. J. Meyer, *J. Phys. Chem. B*, 2010, **114**, 14596–14604.
22 U. B. Cappel, S. M. Feldt, J. Schöneboom, A. Hagfeldt and G. Boschloo, *J. Am. Chem. Soc.*, 2010, **132**, 9096–9101.
23 C. J. Barbé, F. Arendse, P. Comte, M. Jirousek, F. Lenzmann, V. Shklover and M. Grätzel, *J. Am. Ceram. Soc.*, 1997, **80**, 3157–3171.
24 S. Ito, P. Chen, P. Comte, M. K. Nazeeruddin, P. Liska and M. Gra, *Prog. Photovoltaics*, 2007, **15**, 603–612.
25 X. Jiang, K. M. Karlsson, E. Gabrielsson, E. M. J. Johansson, M. Quintana, M. Karlsson, L. Sun, G. Boschloo and A. Hagfeldt, *Adv. Funct. Mater.*, 2011, **21**, 2944–2952.
26 R. Zhu, C.-Y. Jiang, B. Liu and S. Ramakrishna, *Adv. Mater.*, 2009, **21**, 994–1000.
27 H. J. Snaith, R. Humphry-Baker, P. Chen, I. Cesar, S. M. Zakeeruddin and M. Grätzel, *Nanotechnology*, 2008, **19**, 424003.
28 P. Docampo, A. Hey, S. Guldin, R. Gunning, U. Steiner and H. J. Snaith, *Adv. Funct. Mater.*, 2012, **22**, 5010–5019.

